

A SHORT REVIEW OF ABLATIVE-MATERIAL RESPONSE MODELS AND SIMULATION TOOLS

J. Lachaud¹, T. E. Magin², I. Cozmuta³, and N. N. Mansour⁴

¹Univ. California Santa Cruz/UARC, 94035 Moffett Field, CA, USA

²von Karman Institute, B-1640 Rhode-Saint-Genèse, Belgium

³ERC/NASA ARC, 94035 Moffett Field, CA, USA

⁴NASA Ames Research Center, 94035 Moffett Field, CA, USA

ABSTRACT

A review of the governing equations and boundary conditions used to model the response of ablative materials submitted to a high-enthalpy flow is proposed. The heritage of model-development efforts undertaken in the 1960s is extremely clear: the bases of the models used in the community are mathematically equivalent. Most of the material-response codes implement a single model in which the equation parameters may be modified to model different materials or conditions. The level of fidelity of the models implemented in design tools only slightly varies. Research and development codes are generally more advanced but often not as robust. The capabilities of 25 codes along with research and development efforts currently in progress are summarized in a color-coded table.

Key words: Ablative material; modeling; design tool.

NOMENCLATURE

Latin

A_i	Gaseous species i
A_j	Arrhenius law pre-exponential factor, SI
C_H	Stanton number for heat transfer
C_M	Stanton number for mass transfer
c_p	Specific heat, $J \cdot kg^{-1} \cdot K^{-1}$
e	Specific energy, $J \cdot kg^{-1}$
E_j	Arrhenius law activation energy, $J \cdot kg^{-1}$
\mathcal{F}_i	Diffusion flux of the i^{th} species, $kg \cdot m^{-2} \cdot s^{-1}$
F_j	Fraction of mass lost through pyrolysis reaction j
Fo	Forchheimer number
h	Specific enthalpy, $J \cdot kg^{-1}$
j	Diffusive flux, $mol \cdot m^{-2} \cdot s^{-1}$
K	Permeability
K_i	Chemical equilibrium constant for reaction i
l	Thickness or length, m
\dot{m}	Mass flow rate, $kg \cdot m^{-2} \cdot s^{-1}$
m_j	Arrhenius law parameter
M_k	Molar mass of species k , $kg \cdot mol^{-1}$
N_g	Number of gaseous species
n_j	Arrhenius law parameter

N_p	Number of pyrolysis reactions
p	Pressure, Pa
q	Heat flux, $J \cdot m^{-2} \cdot s^{-1}$
R	Perfect gas constant, $J \cdot kg^{-1} \cdot K^{-1}$
v	Convection velocity, $m \cdot s^{-1}$
y	Mass fraction

Greek

β	Klinkenberg coefficient, Pa
ϵ	Volume fraction
γ_{ji}	Stoichiometric coefficient, reaction j species i
μ	Viscosity, $Pa \cdot s^1$
ω	Reaction rate, $mol \cdot m^{-3} \cdot s^{-1}$
ω^s	Solid reaction rate, $mol \cdot m^{-3} \cdot s^{-1}$
Π	Pyrolysis gas production rate, $kg \cdot m^{-3} \cdot s^{-1}$
π	Molar pyrolysis-gas production rate of species i , $mol \cdot m^{-3} \cdot s^{-1}$
ρ	Density, $kg \cdot m^{-3}$
τ	Characteristic time, s
ξ_j	Advancement of pyrolysis reaction j

Subscripts

a	Ablative material (gas, fiber, and matrix)
c	Char
e	Boundary layer edge properties
f	Reinforcement (non-pyrolyzing phase)
g	Gas phase
m, PM	Polymer matrix
mv	Virgin polymer matrix
p	Pyrolysis
pg	Pyrolysis gas
s	Solid phase

Conventions

$\partial_{\mathbf{x}} \cdot ()$	Divergence
$\partial_t ()$	Time derivative
$\underline{\underline{T}}$	Second order tensor
$\underline{\underline{u}}$	Vector

1. INTRODUCTION

During re-entry, a fraction of the heat is transferred to the thermal protection system (TPS) leading to a gradual temperature increase of the material (figure 1). With the temperature increase, the virgin material is successively trans-

formed and removed by two phenomena. The first transformation phenomenon is called pyrolysis. During pyrolysis, the pyrolyzing phase of the material (often a polymer matrix) progressively carbonizes and loses mass producing pyrolysis gases. The pyrolysis gases are transported out of the material by diffusion and convection through the pore network. During this transfer, their chemical composition evolves as their temperature increases. The second transformation phenomenon is the ablation of the char that is composed of the residual carbonized matrix and of the non-pyrolyzing phase (often a carbon or silicon-carbide fibrous preform). Depending on reentry conditions, ablation may be due to heterogeneous chemical reactions (oxidation, nitridation), phase change (sublimation), and/or mechanical erosion (spallation). The main quantities of interest for TPS design are: (1) the peak temperature of the bondline at the interface of the TPS and the substructure and (2) the total surface recession. These two design parameters are predicted by simulation tools specifically developed for ablative materials.

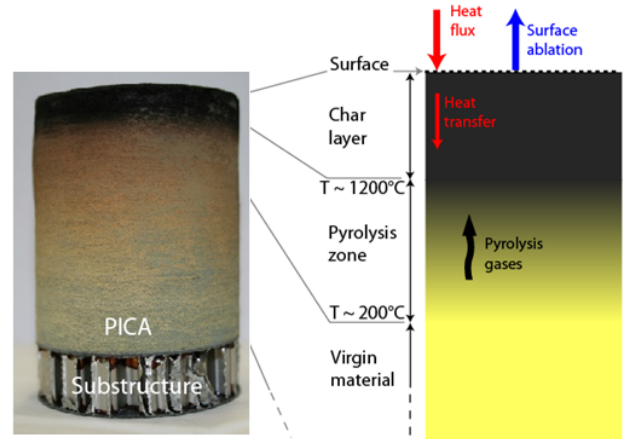


Figure 1. Picture of a core of ablative material extracted from the TPS of Stardust [2] and schematic of the zones of degradation illustrating the material response to a high-enthalpy flow.

2. CONSTITUTIVE MODELS

2.1. Mass conservation

The gaseous mass-conservation equation includes a production term (right-hand side) to account for the pyrolysis gas production, noted Π , and reads

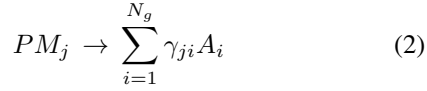
$$\partial_t(\epsilon_g \rho_g) + \partial_x \cdot (\epsilon_g \rho_g \mathbf{v}_g) = \Pi \quad (1)$$

The first open literature publication providing a very detailed and comprehensive analysis of ablative-material response in high enthalpy environments is the Aerotherm report from 1968 describing their suite of design tools [1]. CMA and ACE, Aerotherm's in-depth material response and surface ablation codes respectively, are cited as a reference in most publications in the field. The models implemented in current design-capable tools are mostly replicas (or parallel developments) of the Aerotherm model with slight variations. Interestingly, over the years, the modifications to the Aerotherm model have mainly involved simplifications, with some of the Aerotherm capabilities currently no longer maintained in several major design-tools. Recent interest in manned-rated and challenging design missions (e.g. high mass, very high velocity, porous materials) has raised the need for high-fidelity models capable of providing optimized design and comprehensive uncertainty quantifications. All the capabilities of the Aerotherm's suite of tools and the rich academic work on pyrolysis and ablation are being revisited and progressively introduced (or re-introduced) both in research codes and in design tools. In a complementary effort, several academic, government, and industrial teams are working on the development, the implementation, and the validation of original physics-based models that will enable anchoring of CMA/ACE-based design tools, accurate uncertainty analysis, and maybe become the future base models for design-rated codes. This paper first presents the pyrolysis-ablation problem through the governing equations (mass, momentum, and energy conservation) and boundary conditions. Different levels of modeling fidelity are presented and discussed. An effort was made to gather information on the simulation tools that are actively used either for design or for research and development. The capabilities of each of these codes are summed up in figure 4.

In several codes, the time derivative is omitted and the gas flow problem is treated as a succession of steady state problems (see section 4). This simplification is correct when the variation of the intensive variables (temperature, pressure) are slow compared to the characteristic time of the flow in the porous medium. The characteristic time of the pyrolysis gas flow, τ_{pg} may be defined as the ratio of the thickness of the char layer - l_c - to the velocity of the gas. In typical re-entry applications, $\tau_{pg} = l_c/v_g \simeq 0.01/1 = 0.01s$. Therefore, the omission of the time derivative is an acceptable practice for situations for which the variations of the intensive variables are negligible over time steps of $\tau_{pg} \ll \tau_{step} = 1s$. The determination of the direction of the gas velocity, \mathbf{v}_g , is necessary to solve the average mass-conservation equation. In several one-dimensional codes, this equation is numerically integrated with the assumption that the gas flow is perpendicular to the surface and directed towards the surface. This is exact in one-dimensional steady-state problems with an impermeable back face. In other conditions and in multi-dimensional problems, the direction of the flow has to be determined by resolution of the momentum-conservation equation (see subsection 2.2).

The pyrolysis gas production is obtained by fitting thermogravimetry analysis of the resin decomposition using one or several Arrhenius laws [3]. For example, for phenolic polymers, it has been shown that the pyrolysis degradation process follows four steps [4], that may be de-

scribed by four heterogeneous decomposition reactions [5]. A convenient notation for $j \in [1, N_p]$ pyrolysis reactions is



where PM_j is a fictive solid species of the pyrolysing polymer matrix (PM). The pyrolysing matrix density is then given by

$$\epsilon_m \rho_m = \epsilon_{mv} \rho_{mv} \sum_{j=1}^{N_p} F_j (1 - \xi_j) \quad (3)$$

where

$$\frac{\partial_t \xi_j}{(1 - \xi_j)^{m_j}} = T^{n_j} A_j \exp\left(-\frac{E_j}{RT}\right) \quad (4)$$

The pyrolysis-gas production is given by

$$\Pi = -\partial_t(\epsilon_m \rho_m) = \epsilon_{mv} \rho_{mv} \sum_{j=1}^{N_p} F_j \partial_t(\xi_j) \quad (5)$$

In the literature, the equations used to describe pyrolysis models vary but they are mathematically equivalent.

It is important to mention that state-of-the-art design codes do not track the species production. Only the average mass production $-\Pi$ is computed from the Arrhenius laws. A constant elemental fraction of the pyrolysis gas is assumed. The gas chemical composition and derived quantities (gas enthalpy, viscosity, mean molar mass) are then computed using the chemical equilibrium assumption or heuristic methods.

The pyrolysis gas production rate for each species i could readily be obtained using

$$\pi_i = \epsilon_m \rho_{mv} \sum_{j=1}^{N_p} [\partial_t \xi_j F_j \tilde{\gamma}_{ji}] \quad (6)$$

where

$$\tilde{\gamma}_{ji} = \frac{\gamma_{ji}}{\sum_{k=1}^{N_g} \gamma_{jk} \mathcal{M}_k} \quad (7)$$

This requires the experimental determination of the stoichiometric factors $-\gamma_{ji}$, which are not directly available in the literature but may be derived from experimental studies [4–6]. The overall pyrolysis gas production may still be obtained from: $\Pi = \sum_{i=1}^{N_s} [\pi_i M_i]$.

Higher fidelity models are being developed and implemented. They account for species production, transport, and chemical reactions (finite-rate chemistry) within porous media. The species conservation equation may be written in mass fraction $-y_i$ as

$$\partial_t(\epsilon_g \rho_g y_i) + \partial_{\mathbf{x}} \cdot (\epsilon_g \rho_g y_i \mathbf{v}_g) + \partial_{\mathbf{x}} \cdot \mathcal{F}_i = \pi_i M_i + \epsilon_g \omega_i M_i \quad (8)$$

Both pyrolysis species production $-\pi_i$ and chemical species production $-\omega_i$ are needed. Currently, for the computation of ω_i , the finite-rate chemistry model developed by Pike and April in the late 1960s [7, 8] is used for preliminary analyses. The model was developed using chemical data and experimental techniques available at that time. Efforts are being undertaken by several teams to develop finite-rate chemistry models based on new data and design modern experimental setups for the validation of global mechanisms [9]. \mathcal{F}_i is the diffusion flux of the i^{th} species. At low pressures, mass transfer (diffusion) in porous media is not negligible compared to advection [10]. Mass transfer in porous media is a complex problem. The effective diffusion coefficient is smaller than the bulk diffusion coefficient due to tortuosity effects [10, 11]. A popular extension to porous media of the Stefan-Maxwell model for bulk multi-component diffusion [12] is the *dusty gas model* [11]. To our knowledge no ablation material-response code has such a capability yet.

The solid-phase mass conservation is also integrated to compute the effective density of the solid. The volume-averaged density change of the matrix (due to pyrolysis $-\Pi$) is currently modeled using forms equivalent to

$$\partial_t(\epsilon_m \rho_m) = -\Pi \quad (9)$$

which is easily derived from equation 5. The current assumption is that there is no ablation or coking in-depth. Coking is neglected and ablation is modeled as a surface phenomenon only. Therefore, ablation is accounted for using a prescribed recession velocity at the wall, handled as a boundary condition (rather than as an in-depth constitutive equation) as described in section 3.

Current research efforts aim at developing models for in-depth coking and ablation. For this application, the solid mass-conservation equation may be generalized to account for heterogeneous reactions

$$\partial_t(\epsilon_s \rho_s) = \partial_t(\epsilon_m \rho_m + \epsilon_f \rho_f) = -\Pi + \sum_{i \in s} \epsilon_g \omega_i^s M_i \quad (10)$$

However, the determination of the intrinsic heterogeneous reaction rates $-\omega_i^s$ is not an easy task and is still being investigated [9].

2.2. Momentum conservation in porous media

The average gas velocity is obtained by resolution of the momentum-conservation equation. In porous media, the

volume-averaged momentum conservation may be written as

$$\mathbf{v}_g = -\frac{1}{\epsilon_g \mu} \frac{1 + \beta/p}{1 + Fo} \underline{\underline{\mathbf{K}}} \cdot \partial_{\mathbf{x}} p \quad (11)$$

Most of the materials are anisotropic, therefore, the permeability - $\underline{\underline{\mathbf{K}}}$ - is a second order tensor. For example, Fiberform, the carbon preform of PICA [13], has orthotropic permeability properties [14]. For creeping (Stokes) flows in the continuum regime (in the pores of the material), the volume-average momentum conservation degenerates into Darcy's law ($\beta = 0$, $Fo = 0$). The term $1 + \beta/p$ is the Klinkenberg correction to account for slip effects (at the pore scale) when the Knudsen number (ratio of the mean free path to the mean pore diameter) is not small. The term $1 + Fo$ is the Forchheimer correction to account for high velocity effects at the pore scale (flow separation in the continuum regime). Typically, Forchheimer effects are expected to occur for pyrolysis gas velocities higher than 50 m/s (that is, in high-density ablative materials submitted to very high heat fluxes). It is not advised to use both corrections simultaneously as they address different regimes.

2.3. Energy conservation

According to Puiroux [15], solid and gas phases are in thermal equilibrium as long as the Péclet number for diffusion of heat within the pores is small ($Pe = \epsilon_g \rho_g c_{p,g} d_p v_g / k_g$). In most of the applications of interest for space agencies, the small pore size ($< 100 \mu\text{m}$) and the slow pyrolysis gas flow ($v_g \sim 1 \text{ m/s}$) insure a small Péclet number: the gas temperature accommodates to the solid temperature within the pores [10]. Under the thermal equilibrium assumption, the energy conservation may be written as

$$\begin{aligned} \partial_t \rho_a e_a + \partial_{\mathbf{x}} \cdot (\epsilon_g \rho_g h_g \mathbf{v}_g) + \partial_{\mathbf{x}} \cdot \sum_{i=1}^{N_g} (h_i \mathcal{F}_i) \\ = \partial_{\mathbf{x}} \cdot (\underline{\underline{\mathbf{k}}} \cdot \partial_{\mathbf{x}} T) + \mu \epsilon_g^2 (\underline{\underline{\mathbf{K}}}^{-1} \cdot \mathbf{v}) \cdot \mathbf{v} \end{aligned} \quad (12)$$

where the total (storage) energy of the ablative material is the sum of the energy of its components

$$\rho_a e_a = \epsilon_g \rho_g e_g + \epsilon_m \rho_m h_m + \epsilon_f \rho_f h_f \quad (13)$$

The second and third terms of the left-hand side are the energy convected (advection) and the energy transferred (diffusion) by the pyrolysis gases, respectively. Heat transfer is conveniently modeled as an effective diffusive transfer (Fourier's law). The effective conductivity - $\underline{\underline{\mathbf{k}}}$ - is a second order tensor accounting for conduction in the solid, conduction in the gas, and effective radiative heat transfer. The validity of this effective (volume-averaged)

approach is questionable. The main issue is the validity of the linearization of the radiative heat transfer. A theoretical study has shown that radiative heat transfer may be linearized for two-dimensional carbon-fiber preforms [16, 17]. The applicability to other materials is not straightforward and needs to be investigated. The second term on the right-hand side is the energy dissipated by viscous effects in Darcian regime [18]. It is small compared to the heat transfer term and often neglected.

3. BOUNDARY CONDITIONS

At the bondline, conservative boundary conditions are generally used (adiabatic and impermeable). At the wall and in ablative conditions, surface energy balance and surface mass balance are used as boundary conditions. [Of course, simple wall boundary conditions may always be used for simple analyses, e.g. fixed temperature.]

3.1. Surface energy balance

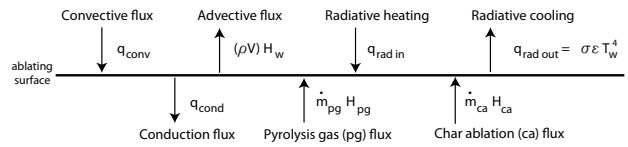


Figure 2. Energy balance at the wall

The surface energy balance at the wall depicted in figure 2 reads

$$q_{conv} - (\rho V)h_w + q_{rad,in} - q_{rad,out} - q_{cond} + \dot{m}_{pg}h_{pg} + \dot{m}_{ca}h_{ca} = 0 \quad (14)$$

where the convective heat flux - $q_{conv} = \rho_e u_e C'_H (h_e - h_w)$ - and the radiative heat flux are extracted from CFD simulations. The Stanton number C'_H is corrected to account for the blockage induced by the pyrolysis-ablation gas-blowing; that is, the heat transfer coefficient is corrected. For example, the following correction is widely used $C'_H = C_H \ln(1 + 2\lambda B') / \ln(2\lambda B')$, where $B' = (\dot{m}_{pg} + \dot{m}_{ca}) / (\rho_e u_e C_M)$ is a dimensionless mass flow rate and λ is a scaling factor usually taken equal to 0.5 [19]. The resolution of Eq. 14 requires the evaluation of the pyrolysis-gas flow rate - \dot{m}_{pg} - and of the ablation rate - \dot{m}_{ca} .

3.2. Surface mass balance and recession rate

The pyrolysis-gas flow rate - \dot{m}_{pg} - is directly obtained in the material-response code by integration of the pyrolysis, transport, and mass equations, as explained previously. However, the ablation rate - \dot{m}_{ca} - is a function of both the mass transfer in the boundary layer and the thermochemical properties at the wall (pyrolysis-gas blowing rate and composition, temperature, pressure, boundary-layer

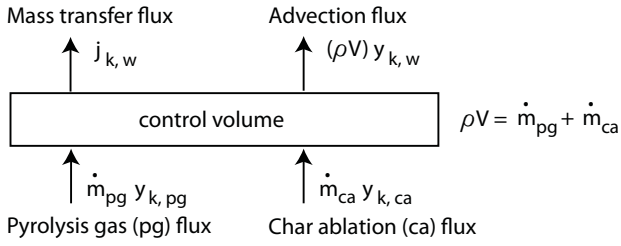


Figure 3. Element mass-fraction conservation at the wall

gas composition). A common practice is to assume thermochemical equilibrium at the wall to compute the ablation rate. The model still in use in the community was developed in the sixties [20]. It is based on element conservation in steady-state in a control volume close to the wall as sketched in figure 3 and expressed in Eq. 15. The underlying hypothesis is that over a time increment Δt , the equilibrium chemistry problem in the control volume is quasi-steady (decoupling of the material response and of the boundary layer problem). This increment Δt should be at least as long as the time increment of the heat transfer simulation (material response code) but short enough so that p , T , \dot{m}_{pg} , and y_{pg} variations may be neglected. This is verified in typical applications. For this presentation, we shall assume equal diffusion coefficients of the elements. Failure modes (spallation, mechanical erosion) are not included and the char is assumed to be composed of a single element (for example, carbon).

The inputs and outputs to this problem are:

- Inputs: \dot{m}_{pg} , $y_{k,pg}$, $y_{k,ca} = 1$, $y_{k,e}$, p , T .
- Outputs: \dot{m}_{ca} , $y_{k,w}$.

The conservation of the mass-fraction of element k in the control volume close the the wall reads:

$$\dot{j}_{k,w} + (\rho V) y_{k,w} = \dot{m}_{pg} y_{k,pg} + \dot{m}_{ca} y_{k,ca} \quad (15)$$

where pg = pyrolysis gases, ca = char ablation products, w = wall (or control volume). The usual element-conservation rules apply:

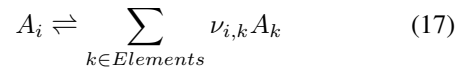
- The relative mass fractions sum to 1 in each phase
 $\sum_k y_{k,w} = 1$; $\sum_k y_{k,pg} = 1$; $\sum_k y_{k,ca} = 1$
- Since p , T are fixed, the element mass-fraction conservation in the control volume is equivalent to the mass conservation.

Under the hypotheses that $Prandtl = Lewis = 1$ and that the diffusion coefficients are equal for the elements, equation 15 may be rewritten as

$$\rho_e u_e C_H (y_{k,w} - y_{k,e}) + (\rho V) y_{k,w} = \dot{m}_{pg} y_{k,pg} + \dot{m}_{ca} y_{k,ca} \quad (16)$$

where, C_H is the Stanton number and $(\rho V) = \dot{m}_{pg} + \dot{m}_{ca}$.

The formation reaction of species A_i may be written:



The i chemical equilibriums read:

$$\sum_{k \in Elements} \nu_{i,k} \ln(x_k) - \ln(x_i) - \ln(K_i) = 0 \quad (18)$$

with $x_i = 1$ if A_i is a solid species. Species mole fractions sum to one:

$$\sum_{i \in Species} x_i = 1 \quad (19)$$

To sum up, the set of equations solved is:

$$\rho_e u_e C_H (y_{k,w} - y_{k,e}) + (\rho V) y_{k,w} = \dot{m}_{pg} y_{k,pg} + \dot{m}_{ca} y_{k,ca} \quad (20)$$

$$\sum_{k \in Elements} \nu_{i,k} \ln(x_k) - \ln(x_i) - \ln(K_i) = 0 \quad (21)$$

with $x_i = 1$ if A_i is a solid species.

$$\sum_{i \in Species} x_i = 1 \quad (22)$$

The base model may be extended when needed to account for multicomponent mass transfer, non-equal diffusion coefficients, failure (spallation, melting), a solid phase made of more than one element (example: SiO_2), corrections to account for heterogeneous finite-rate chemistry. Current development efforts aim at fully modeling the boundary layer and coupling it to material codes, with the recession directly computed in the flow solver.

4. SIMULATION TOOLS

An open-literature search has been done to inventory the simulation tools currently in use or in development for hypersonic re-entry applications. Twenty five codes have been found under the condition that each code should be described in an open-literature document. This condition aims both at protecting intellectual property and keeping the content of this review fully open. Such a search cannot pretend to be fully exhaustive as non-international or internal publications are hard to find, even if they are in the public domain. The name of the codes found and contact information are provided in table 1. The contact listed is either a code developer or a current active user. For each code, one open-literature reference is provided; for most of them, however, many references are available and easily accessible. Our understanding of the current code capabilities and/or development strategies based on open-literature publications are summarized in figure 4. A color-code is used to identify which models (i.e. which equations from the model-review section) are implemented and verified (green), under verification and to be released soon in the official version of the code (yellow), or under implementation (red). The capabilities of the codes are summarized using three criteria, all ranging from on to three: model fidelity (1-3), code dimensionality

Table 1. List of currently available simulation tools

Name	Contact	Owner	Users	Applications	References
Amaryllis	T. van Eekelen	Samtech, Belgium	EADS Astrium, ESA	Design	[21]
CAMAC	W.-S. Lin	CSIST, Taiwan	Taiwan Ins. of Sci. Tech.	Unknown	[22]
CAT	N. N. Mansour	NASA ARC, USA	NASA ARC	Analysis	[23]
CHALEUR	B. Blackwell	SNL, USA	SNL	Design	[24]
CHAP	P. Keller	Boeing, USA	Boeing	Design	[25]
CMA	R. Beck	Aerotherm, USA	NASA, SNL	Design	[26]
CMA/SCMA	C. Park	Tokyo Univ., Japan	JAXA	Design	[27]
CMA/KCMA	P. Reynier	ISA, France	ISA/ESA	Analysis	[28]
CODE-JSC	A. Amar	NASA JSC, USA	NASA	Analysis	[29]
CODE-LaRC	J. Dec	NASA LaRC, USA	NASA LaRC	Analysis	[30]
FABL	J. Merrifield	Fluid Grav. Eng. Ltd., UK	ISA/ESA/FGE	Analysis	[31]
FIAT	Y.-K. Chen	NASA ARC, USA	NASA, SpaceX	Design	[19]
3DFIAT	Y.-K. Chen	NASA ARC, USA	NASA ARC	Analysis	[32]
HERO	M. E. Ewing	ATK, USA	ATK	Analysis	[33]
ITARC	M. E. Ewing	ATK, USA	ATK	Design	[33]
libAblation	R. R. Upadhyay	Univ. of Tex. Aust., USA	UTA	Analysis	[34]
MIG	S. Roy	Univ. of Flo., USA	Univ. of Florida	Analysis	[35]
MOPAR	A. Martin	Univ. of Mich., USA	UKY/Univ. of Michigan	Analysis	[36]
NEQAP	J. B. Scoggins	N. Carol. St. Univ., USA	NCSU	Analysis	[37]
NIDA	G. C. Cheng	Univ. Alab. Birm., USA	UAB	Analysis	[38]
PATO	J. Lachaud	NASA ARC, USA	Univ. Calif. Santa Cruz	Analysis	[39]
STAB	B. Remark	NASA JSC, USA	NASA, FGE	Design	[40]
TITAN	F. S. Milos	NASA ARC, USA	NASA	Analysis	[41]
TMU	A. R. Bahramian	T. Modares Univ., Iran	TMU	Analysis	[42]
US3D	G. Candler	Univ. of Minn., USA	UM	Analysis	[43]

(1-3), and code maturity level (1-3). The model-fidelity range follows the definition of the 4th AF/SNL/NASA Ablation Workshop (1-3 March 2011, Albuquerque, New Mexico): 1: implementation of the CMA model or any mathematically equivalent model; 2: an averaged momentum equation (e.g. Darcy) is added to level-1 models; 3: models of higher fidelity. The code dimensionality refers to the space-dimensionality (of the mesh) and basically refers to: 1: 1-dimension; 2-dimensions (including axis-symmetrical); 3: 3-dimensions. The retained code maturity level is as follows: 1: code verified in limited configurations; 2: codes verified in numerous configurations including both Arc-Jet and Flight conditions; 3: codes used for design. The codes are listed in alphabetical order because providing a classification would be misleading. Indeed, for design purposes, the preference is usually given to codes with a maturity level of 3, while, for analysis, a high fidelity level would be preferred. Finally, in both cases, multi-dimensionality may or may not be critical depending on the application.

5. CONCLUSION

At least twenty five codes are currently in use or in development, with an active community both maintaining state-of-the-art capability and seeking to increase the fidelity of the state-of-the-art model. Design-rated material-response codes currently in use implement an heritage model (from the 1960s) in which the equation parameters may be modified to model different materials or con-

ditions. Research and development codes developed for analysis - at least in a first stage - are generally more advanced but are still under development. Current research efforts undertaken in the community are various and complementary, they include: detailed pyrolysis modeling, finite-rate chemistry mechanism development, mass transport in porous media in rarefied regime, in-depth ablation and coking, radiative heat-transfer analyses, spallation modeling, and boundary layer-material coupling.

ACKNOWLEDGMENTS

This research was partly supported by the Hypersonics Project of the NASA fundamental aeronautics program. Research of T. E. M. is sponsored by the European Research Council Starting Grant #259354.

REFERENCES

1. R. M. Kendall, E. P. Bartlett, R. A. Rindal, and C. B. Moyer. An analysis of the coupled chemically reacting boundary layer and charring ablator: Part I. *NASA CR*, 1060, 1968. 96 p.
2. M. Stackpoole, S. Sepka, I. Cozmuta, and D. Kontinos. Post-flight evaluation of stardust sample return capsule forebody heatshield material. *AIAA paper* 2008-1202, 2008, 12 p.

3. H. W. Goldstein. Pyrolysis kinetics of nylon 6-6, phenolic resin, and their composites. *Journal of macromolecular science, Part A*, 3(4):649–673, 1969.
4. K. A. Trick and T. E. Saliba. Mechanisms of the pyrolysis of phenolic resin in a carbon/phenolic composite. *Carbon*, 33(11):1509–1515, 1995.
5. K. A. Trick, T. E. Saliba, and S. S. Sandhu. A kinetic model of the pyrolysis of phenolic resin in a carbon/phenolic composite. *Carbon*, 35(3):393–401, 1997.
6. G. F. Sykes. Decomposition characteristics of a char-forming phenolic polymer used for ablative composites. *NASA TN*, D-3810, 1967. 20 p.
7. R. W. Pike, G. C. April, and E. G del Valle. Non-equilibrium flow and the kinetics of chemical reactions in the char zone. *NASA status report - Grant NGR 19-001-016*, 1967. 96 p.
8. G. C. April. *Energy transfer in the char zone of a charring ablator*. PhD thesis, Louisiana State University, 1969. Also, NASA CR 107533.
9. J. Lachaud, N. N. Mansour, A. Ceballos, D. Pejakovic, L. Zhang, and J. Marschall. Validation of a volume-averaged fiber-scale model for the oxidation of a carbon-fiber preform. *AIAA Paper 2011-2223*, 2011.
10. J. Lachaud, I. Cozmuta, and N. N. Mansour. Multi-scale approach to ablation modeling of phenolic impregnated carbon ablators. *Journal of Spacecraft and Rockets*, 47(6):910–921, 2010.
11. E. A. Mason and A. P. Malinauskas. *Gas transport in porous media: the dusty-gas model*. Chemical engineering monographs, Elsevier, Amsterdam, 1983.
12. V. Giovangigli. *Multicomponent flow modeling*. Birkhäuser, Boston, 1999.
13. H. K. Tran, C. E. Johnson, D. J. Rasky, F. C. L. Hui, M.-T. Hsu, T. Chen, Y. K. Chen, D. Paragas, and L. Kobayashi. Phenolic impregnated carbon ablators (pica) as thermal protection systems for discovery missions. Technical Report 110440, NASA Technical Memorandum, 1997.
14. J. Marschall and F. S. Milos. Gas permeability of rigid fibrous refractory insulations. *Journal of Thermophysics and Heat Transfer*, 12:528–535, 1998.
15. N. Puiroux, M. Prat, and M. Quintard. Non-equilibrium theories for macroscale heat transfer: ablative composite layer system. *International Journal of Thermal Sciences*, 43:541–554, 2004.
16. T. van Eckelen and J. Lachaud. Radiation heat-transfer model for the ablation zone of low-density carbon-resin composites. *AIAA paper 2010-4904*, 2010.
17. T. van Eckelen and J. Lachaud. Numerical validation of an effective radiation heat transfer model for fiber preforms. *Journal of Spacecraft and Rockets*, in the press, to appear 2011. Engineering note.
18. H. J. Ene and E. Sanchez-Palencia. On thermal equation for flow in porous media. *International Journal of Engineering Science*, 20:623–630, 1982.
19. Y. K. Chen and F. S. Milos. Ablation and thermal response program for spacecraft heatshield analysis. *Journal of Spacecraft and Rockets*, 36(3):475–483, 1999.
20. C. B Moyer and M. R. Wool. Aerotherm equilibrium surface thermochemistry computer program - version 3. Technical report, Aerotherm, April 1970. AD875385.
21. T. van Eckelen, J.-M. Bouilly, S. Hudrisier, J.-M. Dupillier, and Y. Aspa. Design and numerical modelling of charring material ablators for re-entry applications. In *Proceedings of the Sixth European Workshop on Thermal Protection Systems and Hot Structures*, University Stuttgart, Germany, 21-25 November 2009. European Space Agency - WPP-319.
22. W.-S. Lin. Quasi-steady solutions for the ablation of charring materials. *International Journal of Heat and Mass Transfer*, 50:1196–1201, 2007.
23. N. N. Mansour, J. Lachaud, T. E. Magin, J. de Muelenaere, and Y.-K. Chen. High-fidelity charring ablator thermal response model. *AIAA Paper 2011-xxx*, to appear.
24. R. Bond, D. Potter, D. Kuntz, A. Amar, and J. Smith. Aerothermal capabilities at sandia national laboratories. Technical report, Approved for unlimited release as SAND 2005-4513P, 2005.
25. L. B. Hillberg. The convective heating and ablation program (chap). Technical report, Boeing Report No. D2-36402-1, 1966.
26. Aerotherm Inc. Aerotherm charring material thermal response and ablation program - version 3. Technical report, Aerotherm report UM-70-14, 1970.
27. Hyo-Keun Ahn, Chul Park, and Keisuke Sawada. Response of heatshield material at stagnation point of pioneer-venus probes. *Journal of Thermophysics and Heat Transfer*, 16(3):432–439, July-September 2002.
28. P. Reynier. Numerical rebuilding of graphite ablative test case using kcma. In *Proceedings of the Sixth European Workshop on Thermal Protection Systems and Hot Structures*, University Stuttgart, Germany, 21-25 November 2009. European Space Agency - WPP-319.
29. A. J. Amar, N. D. Calvert, and B. S. Kirk. Development and verification of the charring ablating thermal protection implicit system solver. *AIAA paper 2011-144*, 2011.
30. J. A. Dec and R. D. Braun. Ablative thermal response analysis using the finite element method. *AIAA paper 2009-259*, 2009.
31. A. J. Smith. Fabl3, a program for analysing charring ablation thermal protection systems. Technical report, Fluid Gravity Engineering TN20/96 Issue 3, 2000.

32. Y. K. Chen and F. S. Milos. Three-dimensional ablation and thermal response simulation system. AIAA paper 2005-5064, 2005, 15p.
33. M. E. Ewing and D. E. Richardson. Phenomena and material property requirements for a combined structural and thermal ablation model. In *Proc. 4th AF/SNL/NASA Ablation Workshop*, Albuquerque, New Mexico, March 2011.
34. R. R. Upadhyay, P.T. Bauman, R. Stogner, K. W. Schulz, and O. A. Ezekoye. Steady-state ablation model coupling with hypersonic flow. AIAA paper 2010-1176, 2010.
35. A. Bhatia and S. Roy. Pyrolysis gas flow in thermally ablating media using time-implicit discontinuous Galerkin methods. *AIAA paper*, 2011-145, 2011. 15 p.
36. A. Martin and I. Boyd. Simulation of pyrolysis gas within a thermal protection system. AIAA paper 2008-3805, 2008.
37. J. B. Scoggins. The development of a thermochemical nonequilibrium ablation and pyrolysis model for carbon-phenolic thermal protection systems. Master's thesis, North Carolina State University, Raleigh, North Carolina, May 2011.
38. B. S. Venkatachari, G. C. Cheng, R. P. Koomullil, and A. Ayasoufi. Computational tools for re-entry aerothermodynamics: Part II. Surface ablation. AIAA paper 2008-1218, 2008.
39. J. Lachaud and N. N. Mansour. A pyrolysis and ablation toolbox based on openfoam - with application to material response under high-enthalpy environments. In *5th OpenFOAM Workshop*, Gothenburg, Sweden, June 2010. Chalmers University.
40. D. M. Curry. An analysis of a charring ablation thermal protection system. Technical report, NASA TN D-3150, 1965.
41. F. S. Milos and Y. K. Chen. Two-dimensional ablation, thermal response, and sizing program for pyrolyzing ablaters. AIAA paper 2008-1223, 2008.
42. A. R. Bahramian, M. Kokabi, M. H. Navid Famili, and M. H. Beheshty. Ablation and thermal degradation behaviour of a composite based on resol type phenolic resin: Process modeling and experimental. *Polymers*, 47:3661–3673, 2006.
43. R. Gosse and G. Candler. Ablation modeling of electro-magnetic launched projectile for access to space. AIAA paper 2007-1210, 2007.

Code capabilities	A M A R Y L L I S	C A M A C	C A T	C H A L E U R	C H A P	C M A	C M A S	C M A K	C O D E - J S C	C O D E - L a R C	F A B L	F I A T	3 D F I A T	H E R O	I T R A C	L I B A B L A T	M I G	M O P A R	N E Q A P	N I D A	P A T O	S T A B	T I T A N	T M U	U S 3 D M O D
Green : verified and available																									
Yellow : under verification, not in the official version/ release																									
Red : in development																									
Summary																									
Model fidelity (1-3)	2	1	3	2	1	1	2	1	2	1	2	1	1	2	2	1	2	2	2	3	3	1	1	1	1
Code dimensionality (nD= 1-3)	3	1	1	1	1	1	1	1	3	1	1	1	3	3	1	1	1	1	1	1	3	1	2	1	1
Code maturity level (1-3)	3	1	2	3	3	3	3	2	2	2	2	3	2	2	3	1	1	2	1	1	2	3	2	2	1
Gas-phase Mass Conservation	In-depth : Eq. 1																								
Storage ($\partial_t \dots$)	Red		Green	Green					Green			Yellow	Yellow				Green	Green	Green	Green	Green				Green
Divergence ($\partial_x \dots$)	Green	Green	Green	Green	Green	Green	Green	Green	Green	Green	Green	Green	Green	Green	Green	Green	Green	Green	Green	Green	Green	Green	Green	Green	Green
Pyrolysis production (Π)	Green	Green	Green	Green	Green	Green	Green	Green	Green	Green	Green	Green	Green	Green	Green	Green	Green	Green	Green	Green	Green	Green	Green	Green	Green
Pyrolysis model	In-depth: Eq. 2-7																								
SoA Arrhenius laws ($\rightarrow \Pi$)	Green	Green	Green	Green	Green	Green	Green	Green	Green	Green	Green	Green	Green	Green	Green	Green	Green	Green	Green	Green	Green	Green	Green	Green	Green
Species production ($\rightarrow \pi_i$)			Green																	Yellow	Yellow				
Gas-species Conservation	In-depth: Eq. 8																								
Storage ($\partial_t \dots$)			Green																Green	Green	Green				
Divergence ($\partial_x \dots$)			Green																Green	Green	Green				
Multi-component diffusion ($\partial_x F$)			Red																		Red				
Finite-rate chemistry (π_i, ω_i)			Yellow																Green	Green	Green				
Solid-phase mass conservation	In-depth: Eq. 9-10																								
Pyrolyzing matrix mass loss	Green	Green	Green	Green	Green	Green	Green	Green	Green	Green	Green	Green	Green	Green	Green	Green	Green	Green	Green	Green	Green	Green	Green	Green	Green
In-depth ablation/coking			Red																		Yellow				
Momentum conservation	In-depth: Eq. 11																								
Darcy's law	Green		Green	Green		Yellow	Green		Green			Yellow	Yellow	Green	Green	Green	Yellow	Green	Green	Green	Green	Green	Green	Green	Green
Klinkenberg			Red						Green				Yellow								Yellow				
Forchheimer			Red	Green					Green				Yellow					Green							
Energy conservation	In-depth: Eq. 12-13																								
Storage ($\partial_t \dots$)	Green	Green	Green	Green	Green	Green	Green	Green	Green	Green	Green	Green	Green	Green	Green	Green	Green	Green	Green	Green	Green	Green	Green	Green	Green
Divergence ($\partial_x \dots$)	Green	Green	Green	Green	Green	Green	Green	Green	Green	Green	Green	Green	Green	Green	Green	Green	Green	Green	Green	Green	Green	Green	Green	Green	Green
Effective conduction	Green	Green	Green	Green	Green	Green	Green	Green	Green	Green	Green	Green	Green	Green	Green	Green	Green	Green	Green	Green	Green	Green	Green	Green	Green
Viscous dissipation			Yellow	Green														Green	Green		Yellow	Yellow			
Boundary conditions	At the wall: Eq. 14-22																								
Surface energy balance	Green	Green	Green	Green	Green	Green	Green	Green	Green	Green	Green	Green	Green	Green	Green	Green	Green	Green	Green	Green	Green	Green	Green	Green	Green
Wall chemistry from B' table	Green			Green	Green	Green	Green	Green	Green	Green	Green	Green	Green	Green	Green	Green	Green	Green	Green	Green	Green	Green	Green	Green	Green
Internal wall chemistry solver			Yellow										Yellow	Yellow							Yellow	Yellow			
Other utilities	Integrated libraries																								
Equilibrium chemistry solver			Yellow						Green									Yellow			Yellow	Yellow			Yellow
Integrated boundary layer code			Red																		Red				
Script-coupling to CFD code			Red									Yellow	Red					Green			Red		Yellow		

Figure 4. Simulation-tool list and capabilities. [The authors wish to apology for any missing or incorrect information contained in this figure. Corrections and addenda will be greatly appreciated.]